

# Accelerating F-doping in transparent conducting F-doped SnO<sub>2</sub> films for electrochromic energy storage devices

Myeong-Hun Jo<sup>a,1</sup>, Bon-Ryul Koo<sup>b,1</sup>, Hyo-Jin Ahn<sup>a,b,\*</sup>

<sup>a</sup> Department of Materials Science and Engineering, Seoul National University of Science and Technology, Seoul, 01811, South Korea

<sup>b</sup> Program of Materials Science & Engineering, Convergence Institute of Biomedical Engineering and Biomaterials, Seoul National University of Science and Technology, Seoul, 01811, South Korea



## ARTICLE INFO

### Keywords:

Films  
Optical properties  
Electrical properties  
Transition metal oxides  
Electrochromic energy storage performances

## ABSTRACT

In this study, we designed a unique method for increasing F-doping concentration in F-doped SnO<sub>2</sub> (FTO) films, without the extra addition of NH<sub>4</sub>F as a doping source, using NaOH acting as a functional additive during ultrasonic spray pyrolysis. The NaOH triggers a chemical reaction with HF, resulting in the presence of dissociated F<sup>-</sup> acting as a doping source. To optimize the NaOH effect on the transparent conducting performance in the FTO films, we adjusted the volume percentages of the NaOH to 0, 1, 5, and 10 vol% during FTO deposition. Compared with other FTO films, the FTO film prepared with 5 vol% NaOH revealed enhanced carrier concentration ( $7.81 \times 10^{20} \text{ cm}^{-3}$ ) generated by the increased F-doping concentration (3.57 at%) and high Hall mobility ( $27.18 \text{ cm}^2/(\text{V S})$ ) through smooth surface morphology. Such behaviors through the NaOH effect resulted in FTO films with decreased sheet resistance ( $5.3 \pm 0.16 \Omega/\square$ ), leading to improved electrochromic (EC) energy storage performances of fast switching speed (6.6 s for coloration speed and 8.4 s for bleaching speed) due to faster electrochemical kinetics at the active electrodes, high coloration efficiency ( $58.1 \text{ cm}^2/\text{C}$ ) and high specific capacitance ( $65.2 \text{ F/g}$  at  $2 \text{ A/g}$ ) via enhanced electrochemical activity in the active electrodes that widens the transmittance modulation. Therefore, our study suggests a novel method to improve the transparent conducting performances of FTO films for application in EC energy storage devices.

## 1. Introduction

Technological advances in energy-efficient devices like lithium-ion batteries, solar cells, electrochemical capacitors, and electrochromic (EC) devices, have been studied by many researchers to overcome challenges of energy exhaustion and environmental pollution. Among these, the EC devices can save energy or increase energy-efficiency by conditioning the solar energy entering a building by controlling the optical properties (transmittance, absorption, and color) of materials using applied external biases [1,2]. In addition, the operating mechanism of the EC devices is based on the insertion/extraction of charges in active materials, which is similar to the concept of energy-storage. Consequently, recent studies focused on the integration of EC functionality and energy-storage for multifunctional applications that can monitor stored energy levels to manage variations in a noticeable and predictable manner [3–5]. Generally, EC energy storage devices have a sandwich structure with transparent conducting oxide (TCO)/anodic material/electrolyte/cathodic material/TCO. In the device

components, the TCO films with ideal properties of high transmittance (> 80%) and a low resistivity ( $< 10^{-4} \Omega \text{ cm}$ ) play essential roles in the transfer of electrons formed in the active material and guarantee transparency of the devices [6]. Therefore, conductive characteristics of TCO films could directly affect the EC energy storage performances, including coloration efficiency (CE) and specific capacitance, by assisting in the activation of electrochemical reactions in the active materials and by improving the switching speed and rate capability by accelerating the electrochemical kinetics of the electrodes. The realization of these improvements remains as a major research focus with the aim of providing TCO films with satisfactory performance for practical applications [7,8].

Fluorine-doped tin oxide (FTO) is known as familiar TCO in electrochemical applications, such as dye-sensitized solar cells and EC devices, due to its outstanding transparent conducting performance, good thermal and chemical stability, and low element cost [9,10]. In this study, adjustable control of the FTO structure using ultrasonic spray pyrolysis deposition (USPD) has been attempted as a means to generate

\* Corresponding author. Department of Materials Science and Engineering, Seoul National University of Science and Technology, Seoul, 01811, South Korea.

E-mail addresses: [hjahn@seoultech.ac.kr](mailto:hjahn@seoultech.ac.kr), [hjahn@snut.ac.kr](mailto:hjahn@snut.ac.kr) (H.-J. Ahn).

<sup>1</sup> M.-H. Jo and B.-R. Koo contributed equally to this work.

high-performance FTO films [6,11,12]. As a simple process parameter for improving performance of FTO films, increasing deposition time of the USPD leads to a reduced sheet resistance ( $R_{sh}$ ) due to increased carrier concentration, but with a foggy appearance resulting in the poor transmittance due to the serious thickness [6]. Furthermore, Fe co-doping of FTO films has effectively created charge carriers by the introduction of oxygen vacancies that can provide extra two electrons, resulting in the improvement of their transparent conducting performances [11]. However, the intrinsic problem is to be sure that there is a limitation in the incorporation of F ions into  $\text{SnO}_2$  lattice in spite of using rich doping source, resulting in a maximum F-doping concentration of 2.64 at% despite using molar ratio of 1.76 F/Sn. Hence, when amount of  $\text{NH}_4\text{F}$  used as a doping source increases compared to the amount of Sn-based precursors, the FTO films become slightly more conductive, but translucent ( $< \sim 65\%$  for transmittance value) limits their use in functional applications, which is due to redundant crystallite growth from HCl-rich phases formed as a result of incomplete pyrolysis reaction. This is still a major issue to be overcome in FTO fabrication at any cost level [12].

In this stage, we suggest a novel and unique approach to increasing the F-doping in FTO films via the NaOH effect during the USPD. The optimized NaOH effect in forming FTO films improved the dissociation of  $\text{F}^-$ , acting as a doping source from HF in a cooperative interaction with dissociated  $\text{OH}^-$ , resulting in an increase of the F-doping concentration, which is beneficial to high-performance FTO films without the extra consumption of the  $\text{NH}_4\text{F}$  source. In addition, we demonstrated the possibility of improvement in the performance of EC energy storage devices employing FTO films with increased F-doping through the NaOH effect.

## 2. Experimental details

### 2.1. Experimental

Conductive FTO films were invented by optimizing the NaOH contents used as a functional additive to the precursor solution during ultrasonic spray pyrolysis deposition (USPD) on a cleaned glass substrate (Corning EAGLE XG™). To prepare the precursor solution to deposit transparent conducting films, all of solutions were obtained by blending 0.68 M of tin chloride pentahydrate ( $\text{SnCl}_4 \cdot 5\text{H}_2\text{O}$ , SAMCHUN) and 1.20 M of ammonium fluoride ( $\text{NH}_4\text{F}$ , Aldrich) into deionized (DI) water with ethyl alcohol 5 vol% ( $\text{C}_2\text{H}_5\text{OH}$ , Duksan). After stirring, sodium hydroxide (NaOH, SAMCHUN) was additionally subjoined to the clear FTO solutions. The volume percentages of the NaOH to FTO solution were controlled at 0, 1, 5 and 10 vol% to fully optimize the transparent conducting performance of the effected films. USPD was then conducted by allowing the droplets developed from the precursor solution utilizing an ultrasonic atomizer (1.6 MHz) to reach a substrate temperature of 420 °C during the deposition time of 28 min within a fixed length. The other required conditions of the USPD were fixed evenly in the air carrier gas of flow rate for 15 L/min and the rotational speeds of substrates for 5 rpm, thus yielding four types of FTO films using NaOH volume percentages of 0, 1, 5 and 10 vol% (hereafter mentioned to as bare FTO, 1NaOH-FTO, 5NaOH-FTO and 10NaOH-FTO, respectively). To represent the EC energy storage performance using the transparent conducting FTO films, we applied  $\text{WO}_3$  films as an active electrode material. To ready the optimized  $\text{WO}_3$  films, tungsten chloride ( $\text{WCl}_6$ , Aldrich) of 10 wt% was chemically dissolved into 2-propanol ( $(\text{CH}_3)_2\text{CHOH}$ , Aldrich), and the derived sol solution was additionally spin coated for 30 s for 2000 rpm on all FTO films. The spin coating of the sol solution was repeated two times. After that, four types of electrodes composed of  $\text{WO}_3$  films coated on the FTO were obtained by annealing the samples at 300 °C in air.

### 2.2. Characterization

The film crystal structure was determined via X-ray diffraction (Rigaku -Dmax 2500 using  $\text{Cu K}_\alpha$  radiation). The thermal behavior of all FTO solutions was analyzed through differential scanning calorimetry (DSC) measurement from room temperature to 420 °C with a heating ascent rate of 10 °C  $\text{minute}^{-1}$  in air. The surface morphology of the films was imaged using field emission scanning electron microscopy (FESEM, Hitachi S-4800). The chemical bonding states were identified through X-ray photoelectron spectroscopy (ESCALAB 250, Al  $\text{K}_\alpha$  X-ray source). The electrical and optical properties were demonstrated via a Hall effect measurement system (HMS-3000) and ultraviolet–visible (UV–vis) spectroscopy (PerkinElmer, Lambda 35), severally. The electrochemical properties representing EC performances were taken in three electrode setups, consisting of a counter electrode with Pt wire, reference electrode with Ag wire and working electrode with  $\text{WO}_3$  coated FTO films, and 1 M of  $\text{LiClO}_4$  (in propylene carbonate (PC)) electrolyte on a potentiostat/galvanostat (PGSTAT302 N, Metrohm Autolab) in the scan rate of 20 mV/s in  $-0.7$  to 1.0 V range. The EC energy storage performances were measured using an association of a UV–vis spectroscopy and potentiostat/galvanostat. The electrochemical impedance spectroscopy (EIS) measurement was fulfilled on a potentiostat/galvanostat (PGSTAT302 N, Eco Chemie) by appertaining a sinusoidal signal of 10 mV amplitude from 0.1 Hz to 100 kHz of frequency range.

## 3. Results and discussion

Fig. 1a reveals the XRD curves acquired from bare FTO, 1NaOH-FTO, 5NaOH-FTO, and 10NaOH-FTO. Bare FTO exhibits characteristic peaks at 51.72°, 37.98°, 33.84°, and 26.58°, which are well matched to the (211), (200), (101), and (110) planes of tetragonal rutile  $\text{SnO}_2$  (JCPDS no. 88-0287), severally. The diffraction peaks are located at a bit lower position than those of typical  $\text{SnO}_2$  ((211) plane at  $\sim 51.82^\circ$ , (200) plane at  $\sim 38.00^\circ$ , (101) plane at  $\sim 33.90^\circ$ , and (110) plane at  $\sim 26.65^\circ$ ). This indicates that there are substitutions of the larger  $\text{F}^-$  (ionic radius of 0.133 nm) for the smaller  $\text{O}^{2-}$  (0.132 nm) in the  $\text{SnO}_2$ , which is demonstrating the successful formation of FTO phase, as judged from the Bragg's equation ( $n\lambda = 2d\sin\theta$ ) [6,11]. In enlarged XRD curves (Fig. 1b), it is worth noticing that the peak shift of the (200) plane toward a lower angle is gradually generated from bare FTO to 5NaOH-FTO despite the use of same F/Sn molar ratio during the FTO deposition. This indicated an increased incorporation of F ions into  $\text{SnO}_2$  lattice, which can be due to the unique NaOH effect in the pyrolysis reaction as discussed below.

The expanded DSC curves obtained when forming FTO films in the temperature range of 140–420 °C for bare FTO, 1NaOH-FTO, 5NaOH-FTO, and 10NaOH-FTO are shown in Fig. 1c. For bare FTO, there are three characteristic endothermic zones, which are typical pyrolysis reactions in forming FTO phase through the decomposition of  $\text{NH}_4\text{F}$  as the doping source ( $\text{NH}_4\text{F} \rightarrow \text{NH}_3 + \text{HF}$ ) for zone 1 at 160–210 °C, hydrolysis of  $\text{SnCl}_4 \cdot 5\text{H}_2\text{O}$  as the main source ( $\text{SnCl}_4 \cdot 5\text{H}_2\text{O} \rightarrow \text{SnO}_2 + 4\text{HCl} + 3\text{H}_2\text{O}$ ) for zone 2 at 260–310 °C, and crystallization of FTO for zone 3 at above 320 °C [13,14]. In typical FTO films, the substitutions of F ions into  $\text{SnO}_2$  lattice is limited due to the escape of produced HF together with other pyrolysis gases, reducing the availability of F-doping effect. This is the critical reason that an excessive molar ratio of  $\text{NH}_4\text{F}$  (1.50–1.87) compared to Sn-based sources must be used to form high-performance FTO films, as presented previous reports besides this study [6,11,15,16]. Compared to the DSC curve of bare FTO, the results from the films formed using NaOH reveal additional characteristic endothermic peaks (Zone 4) that can be related to the chemical reaction between HF and NaOH in the FTO precursor solution, as follows (Eq. (1)) [17]:



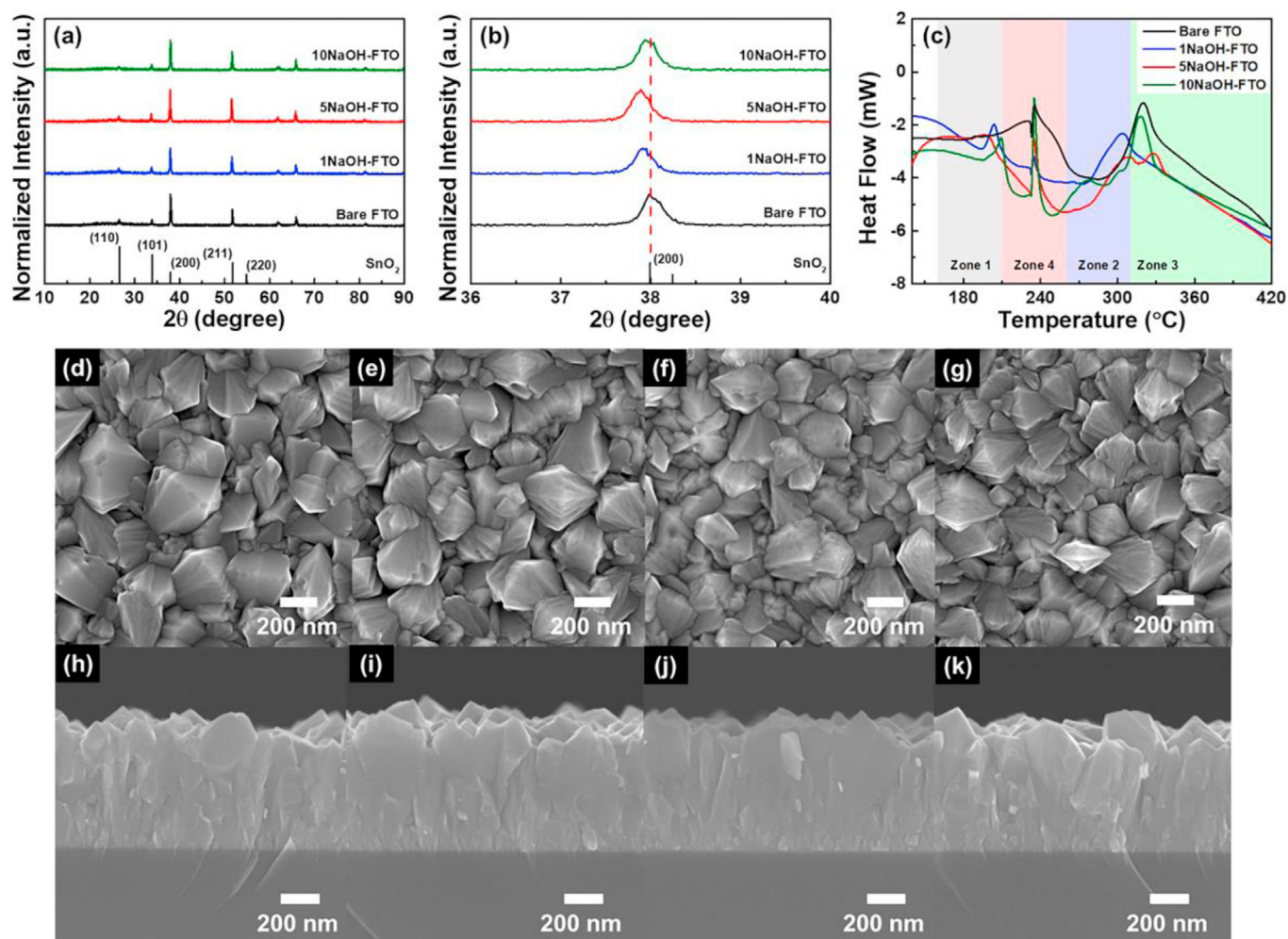


Fig. 1. (a) XRD curves, (b) the magnified curves in the range of 36–40°, and (c) DSC curves of all FTO films, and surface-view and cross-view FESEM images of (d and h) bare FTO, (e and i) 1NaOH-FTO, (f and j) 5NaOH-FTO, (g and k) 10NaOH-FTO.

According to M. E. Guendouzi et al. and Z.-Z. Xie et al., HF is a weak acid, indicating that it does not dissociate completely into  $H^+$  and  $F^-$  in an aqueous solution [18,19]. In contrast, the use of NaOH ( $\rightarrow Na^+ + OH^-$ ) that has dissociated completely in an aqueous solution can induce the accelerated dissociation of  $H^+$  through the reaction with  $OH^-$ , resulting in the presence of dissociated  $F^-$  acting as doping source in the system [18]. Therefore, the NaOH can be suggested as unique media for accelerating F-doping effect in FTO films through the induced dissociation of  $F^-$ . However, for 10NaOH-FTO, there is a relaxation of (200) peak shift in the XRD spectrum compared to 5NaOH-FTO, which may be due to a reaction imbalance between zone 3 and 4, showing the limited hydrolysis of  $SnCl_4 \cdot 5H_2O$  through the excessive effect of the NaOH (see Fig. 1c). This, in turn, reduces the F-doping effect into  $SnO_2$ . Regarding the NaOH effect on surface morphology, the films show the gradual reduction of interlocked polyhedral crystallite sizes from bare FTO (301.48–480.42 nm) to 5NaOH-FTO (260.41–458.72 nm). This reduction can be attributed to the exercise of the compressive stresses during crystallite growth induced due to substitution of  $O^{2-}$  by  $F^-$  relating to acceleration of F-doping effect, thus forming a dense surface structure that is useful for facilitating carrier transport at the surface [20,21]. In addition, it is observed for 10NaOH-FTO that there is reduced crystallites (242.29–436.31 nm) despite relaxation of F-doping effect compared to 5NaOH-FTO, which can be due to resultant pyrolysis gases, such as HCl and  $H_2O$ , being adsorbed on the crystallites to limit crystallite growth [22]. For film thickness, there is no remarkable difference among the films (679.23–720.71 nm for

bare FTO, 687.61–736.95 nm for 1NaOH-FTO, 689.52–730.52 nm for 5NaOH-FTO, and 687.62–735.23 nm for 10NaOH-FTO, see Fig. 2h–k), which indicates that the NaOH has no impact in the rate of the FTO deposition. Therefore, the XRD, DSC, and field emission scanning electron microscopy (FESEM) consequences signify that the NaOH effect can lead to formation of the FTO films with improved F doping and surface densification beneficial to carrier concentration and Hall mobility, respectively, for high-performance FTO films.

To draw chemical binding states of all FTO films with the NaOH effect, the XPS analytics was conducted as shown in Fig. 2a and b. The characteristic peaks of XPS Sn  $3d_{5/2}$  and Sn  $3d_{3/2}$  (see Fig. 2a) are equally emitted at  $\sim 486.7$  and  $\sim 495.2$  eV, respectively, for all films, indicating Sn–Sn bond related to  $Sn^{4+}$  in  $SnO_2$  phase. In addition, release of binding energy occurs at  $\sim 487.85$  eV for Sn  $3d_{5/2}$  and  $\sim 496.4$  eV for Sn  $3d_{3/2}$ , which is a chemical binding state of the Sn–F in agreement with F-doping effect in the  $SnO_2$  phase [20]. Interestingly, it was derived that the area ratio of Sn–F/Sn–Sn gradually increased from bare FTO to 5NaOH-FTO (0.080 for bare FTO, 0.099 for 1NaOH-FTO, and 0.109 for 5NaOH-FTO) with the increase of the NaOH volume percentage as shown in XPS Sn  $3d$  spectra, suggesting a gradual increase of the F-doping concentration in the FTO films (2.64 at% for bare FTO, 3.26 at% for 1NaOH-FTO, and 3.57 at% for 5NaOH-FTO). The variation can have a major impact in optical band gap ( $E_g$ ) of the films, which is determined by the relationship of  $(ah\nu)^2$  versus photon energy ( $h\nu$ ), as the following Eq. (2) [23]:

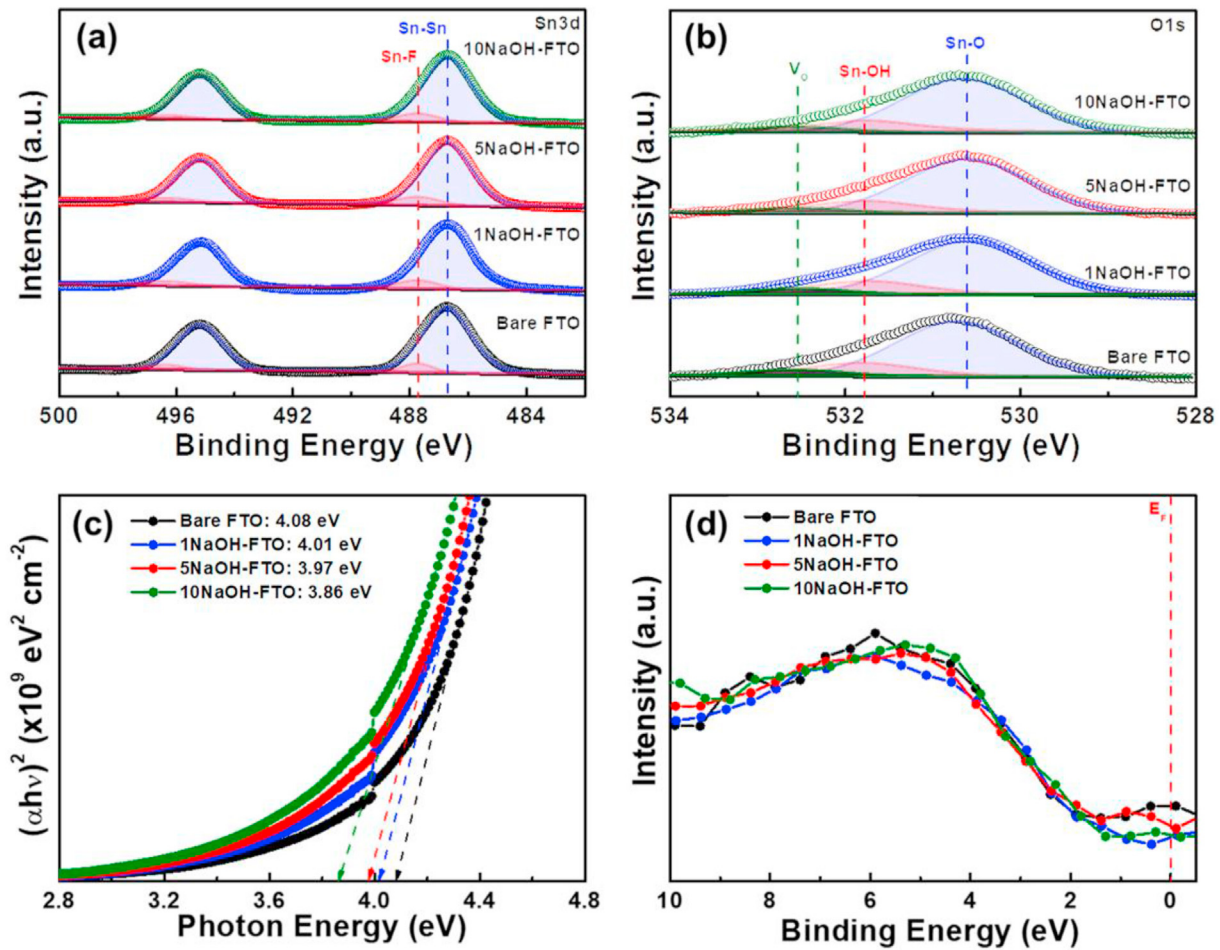


Fig. 2. (a) Sn 3d and (b) O 1s XPS spectra of the FTO films, (c) optical bandgap determined by relationship of the absorption coefficient ( $\alpha$ ) in respect to the incident photon energy ( $h\nu$ ), and (d) valence band spectra of the films.

$$\alpha h\nu = (h\nu - E_g)^n \cdot A \quad (2)$$

here  $\alpha$  is optical absorption coefficient,  $n$  is constant, and  $A$  is energy-independent constant. As shown in Fig. 2c, the calculated  $E_g$  has narrowed behavior from bare FTO to 5NaOH-FTO, which resulted from the merge of the donor band into the conduction band through the increased in F-doping to improve carrier concentration on the FTO films, as confirmed in valence band XPS spectra, showing that there is no variation in position on the valence band maximum (VBM) with different amount of used NaOH (Fig. 2d) [24]. However, 10NaOH-FTO shows a declined area ratio of Sn-F/Sn-Sn (0.098 for 10NaOH-FTO) corresponding to the F-doping concentration of 3.19 at% compared to that of 5NaOH-FTO. The reduced F-doping concentration that occurred despite the use of higher amount of NaOH may be explained by the incomplete hydrolysis of  $\text{SnCl}_4 \cdot 5\text{H}_2\text{O}$ . Hence, a remarkable increase of Sn-OH/Sn-O area ratio is observed in O 1s XPS spectra of 10NaOH-FTO (0.311), as compared with the other films (0.253 for bare FTO, 0.257 for 1NaOH-FTO, and 0.261 for 5NaOH-FTO) (see Fig. 2b), leading to the rapid narrowing of  $E_g$  as a result of the residual Sn-OH phase acting as an impurity band, which is confirmed by the O 1s XPS spectra, which having a bad effect on the carrier concentration in the FTO films [25]. Furthermore, the variation of F-doping effect by the NaOH can be confirmed by the resulting presence of the oxygen vacancy ( $V_o$ ) in the FTO films. The result of calculated  $V_o/\text{Sn-O}$  ratio from the Sn 3d and O 1s XPS spectra shows that the value is gradually decreased from bare FTO (0.084) to 5NaOH-FTO (0.078), which can be attributed to the effect filling the  $V_o$  sites by acceleration of incorporated F ions, hence while there is improved  $V_o$  for 10NaOH-FTO (0.080) [20,22,26].

Therefore, these results indicate that 5NaOH-FTO has an optimal effect, improving the F-doping on  $\text{SnO}_2$ , which makes the utilization of EC energy storage devices possible through the conductive performance of TCO.

Fig. 3a and Table 1 show the electrical properties of all FTO films fabricated by different volume percentage of the NaOH. Their electrical properties, such as resistivity ( $\rho$ ) and sheet resistance ( $R_{sh}$ ), are directly attributed to electrochemical behavior linked to EC energy storage performances. In general, resistivity ( $\rho$ ) of the TCO is substantially dependent on their carrier concentration ( $N$ ) and hall mobility ( $\mu$ ) values. When the volume percentage of the NaOH increases from 0 vol% (bare FTO) to 5 vol% (5NaOH-FTO), the carrier concentration ( $N$ ) value increases from  $5.73 \times 10^{20}$  to  $7.81 \times 10^{20} \text{ cm}^{-3}$  due to increased F-doping [27,28]. However, the 10NaOH-FTO film shows a decreased carrier concentration ( $N$ ) value, which is generated due to the reduction of F-doping effect from the residual Sn-OH phase. While  $\mu$  value is commonly in inverse proportion to the  $N$  in unit volume as the exercise of ingrain carrier scattering [29],  $\mu$  value of the films has increased behavior from  $24.68 \text{ cm}^2/(\text{V s})$  for bare FTO to  $27.18 \text{ cm}^2/(\text{V s})$  for 5NaOH-FTO. This can be explained by the effect to relax the ingrain carrier scattering by the surface densification. However, there is the decreased value on  $22.22 \text{ cm}^2/(\text{V s})$  for 10NaOH-FTO compared to that of 5NaOH-FTO as the result of residual Sn-OH phase resulting in a neutral impurity scattering. Therefore,  $\rho$  values calculated based on these values were revealed to be  $4.52 \times 10^{-4} \Omega \text{ cm}$  for bare FTO,  $3.75 \times 10^{-4} \Omega \text{ cm}$  for 1NaOH-FTO,  $2.94 \times 10^{-4} \Omega \text{ cm}$  for 5NaOH-FTO,  $4.23 \times 10^{-4} \Omega \text{ cm}$  for 10NaOH-FTO, as with the following Eq. (3) [30]:

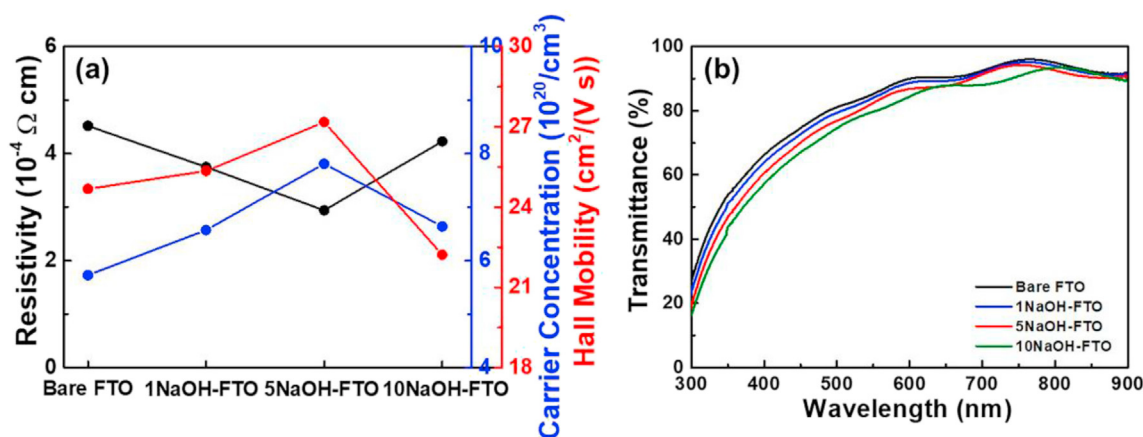


Fig. 3. (a) Plot representing electrical properties with resistivity, carrier concentration, and Hall mobility and (b) optical transmittance curve in wavelength range of 300–900 nm.

Table 1  
Summary of electrical and optical properties measured from all FTO films.

	Bare FTO	1NaOH-FTO	5NaOH-FTO	10NaOH-FTO
Carrier concentration ( $\text{cm}^{-3}$ )	$5.73 \times 10^{20}$	$6.57 \times 10^{20}$	$7.81 \times 10^{20}$	$6.64 \times 10^{20}$
Hall mobility ( $\text{cm}^2/(\text{V s})$ )	24.68	25.35	27.18	22.22
Resistivity ( $\Omega \text{ cm}$ )	$4.52 \times 10^{-4}$	$3.75 \times 10^{-4}$	$2.94 \times 10^{-4}$	$4.23 \times 10^{-4}$
Sheet resistance ( $\Omega/\square$ )	$8.0 \pm 0.27$	$6.8 \pm 0.20$	$5.3 \pm 0.16$	$7.7 \pm 0.28$
Transmittance (%)	84.2	82.0	80.8	78.8

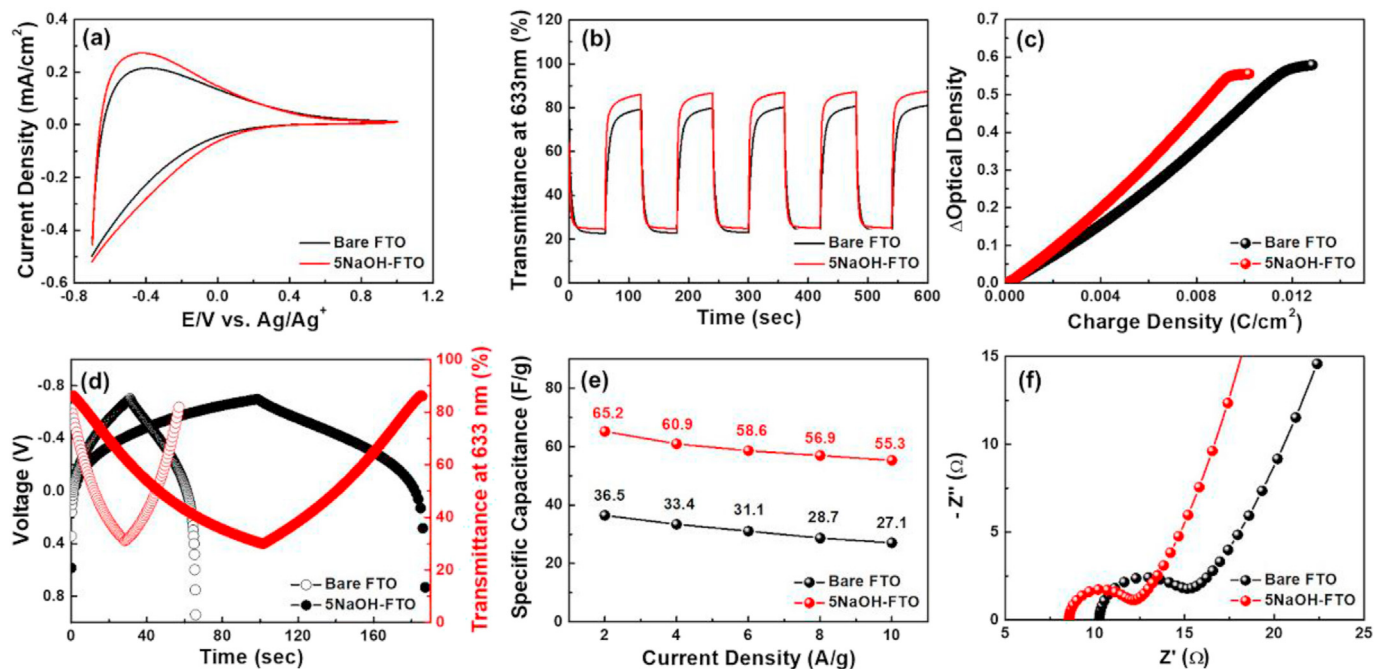


Fig. 4. (a) CV curves traced in potential range from  $-0.7$  to  $1.0$  V at the  $20$  mV/s scan rate, (b) *In situ* optical transmittances curve applied to different potential at  $-0.7$  V for colored state and at  $1.0$  V for bleached state during  $60$  s per each process, (c) OD curve obtained at  $633$  nm, (d) mixed curve of galvanostatic charge/discharging and the following transmittance value, (e) specific capacitances with regard to current densities of  $2, 4, 6, 8,$  and  $10$  A/g, and (f) Nyquist plot in respect to intercalated charge density of  $-0.7$  V.

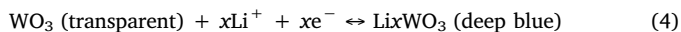
Table 2  
EC energy storage performances of bare FTO and 5NaOH-FTO electrodes.

	Transmittance modulation (% , 633 nm)	Coloration speed (s)	Bleaching speed (s)	CE ( $\text{cm}^2/\text{C}$ )	Specific capacitance (F/g, at 2 A/g)
Bare FTO	56.4	11.0	16.5	38.6	36.5
5NaOH-FTO	61.4	6.6	8.4	58.1	65.2

$$\rho = 1/(\mu eN) \quad (3)$$

here  $\rho$  is resistivity,  $\mu$  is hall mobility,  $e$  is the charge of the electron ( $1.60 \times 10^{-19}$  C) and  $N$  is carrier concentration. In addition, sheet resistance ( $R_{sh}$ ) value obtained by considering measurement volume of the films is  $8.0 \pm 0.27$  for bare FTO,  $6.8 \pm 0.20$  for 1NaOH-FTO,  $5.3 \pm 0.16$  for 5NaOH-FTO,  $7.7 \pm 0.28 \Omega/\square$  for 10NaOH-FTO, suggesting that 5NaOH-FTO possesses a higher electrical property than the other FTO films. The remarkably decreased sheet resistance was mainly resulted from the improvement in both sides of  $N$  and  $\mu$  values owing to the optimized effect of the NaOH in the FTO film, which are caused by the increase of the F-doping concentration and the smooth surface morphology. For optical transmittance of the films, although a slight decrease of the average values from wavelength 300 nm–900 nm is observed in Fig. 3b because of the generation of the ionized donors near the conduction band resulting in the  $E_g$  narrowing, from 84.2% for bare FTO to 78.8% for 10NaOH-FTO, this satisfied the necessary optical property for practical application in optoelectronic devices [25,31]. Therefore, 5NaOH-FTO shows a higher transparent conducting performance as the TCO for EC storage energy devices (Table 1).

Fig. 4a reveals the cyclic voltammetry (CV) characteristic curves of the electrodes coated with  $WO_3$  to trace the electrochemical behavior of bare FTO and 5NaOH-FTO as TCO. The CV curves of entire electrodes emitted a pair of reduction-oxidation peaks related to oxidation at positive potential and reduction in the negative potential of the  $WO_3$ . This redox reaction generates the EC behavior from a transparent film in a bleached state to deep-blue colored film in a colored state through the deintercalation/intercalation of  $Li^+$  and electrons, which can be explained by following Eq. (4) [32,33]:



5NaOH-FTO electrode reveals a greater CV area with increasing current densities for both the anodic and cathodic peaks compared to the bare FTO electrode, which are induced due to the enhancement of electrochemical activity due to a decreased  $R_{sh}$  of the FTO films, which causes the effective transport of large quantity of  $Li^+$  and electrons into the  $WO_3$  films. Therefore, the EC performance characterized by comparing the *in-situ* optical transmittance curves at  $\lambda_{633\text{nm}}$  measured through a co-operation of a double-step chronoamperometry (CA) measurement at the related potential of 1.0 V (bleached state) and  $-0.7$  V (colored state) for 60 s shows that 5NaOH-FTO electrode has a widened transmittance modulation ( $\Delta T = T_b - T_c$ , where  $T_b$  is the transmittance in a bleached state and  $T_c$  is the transmittance in a colored state) of 61.3% and faster switching speeds ( $\tau$ , the time which takes to reach 90% of the loaded transmittance modulation) of 6.6 s for the coloration speed ( $\tau_c$ ) and 8.4 s for the bleaching speed ( $\tau_b$ ), which is a higher value compared to bare FTO electrode showing 56.4% for  $\Delta T$ , 11.0 s for  $\tau_c$ , and 16.5 s for  $\tau_b$  (see Fig. 4b and Table 2). This performance improvement can be defined by effects of increasing electrochemical activity for  $\Delta T$  and the accelerating of  $Li^+$  and electron diffusion for  $\tau$  resulting from the decreased  $R_{sh}$  on the FTO films. In addition, the CE value is considered a comprehensive factor to determine EC performance, which is outlined as the optical density (OD) divided by the intercalated charge densities ( $Q/A$ ) (see Eq. (5) and (6)) [23,34]:

$$CE = \Delta OD / (Q/A) \quad (5)$$

$$\Delta OD = \log (T_b/T_c) \quad (6)$$

where  $Q$  is the charge capacity and  $A$  is the allowed electrode area. As shown in Fig. 4c, the high CE value of the 5NaOH-FTO electrode obtained by sloping the OD curve of 633 nm and the intercalated charge density at  $-0.7$  V indicate that 5NaOH-FTO films can provide optimized EC performance as a TCO, which is because of the generation of widened  $\Delta T$  with effective transport of the  $Li^+$  and electrons in the  $WO_3$  film. By extension, we measured the galvanostatic charge/

discharging to trace the energy storage performances of the FTO films for the devices. With the symmetrical shape of the charging and discharging curve indicating good reversible electrochemical behavior as well as the following variation in transmittance value (see Fig. 4d), it is noted that all specific capacitances of the 5NaOH-FTO electrode measured from 2 to 10 A/g of current densities are higher than bare FTO electrode. This is generated by the reduced  $R_{sh}$  of the FTO film, which is affecting the improvement of electrochemical activity and kinetics at the electrode [2,34–36]. This superb EC energy storage performances were also supported by the electrochemical impedance spectroscopy (EIS) result indicating decreased charge-transfer resistance ( $R_{ct}$ ) through the increase of electrical conductivity of the overall electrodes and series resistance ( $R_s$ ) resulting from the reduced  $R_{sh}$  of the FTO films along with Fig. 4f.

In short, the decreased  $R_{sh}$  of the FTO films through the optimized NaOH effect is beneficial to not only fast switching speeds, which is induced by the efficient electrochemical kinetics of active electrode, but also high CE value and specific capacitance owing to the enhanced electrochemical activity. Therefore, the NaOH effect to increasing F-doping in FTO films can be suggested as an effective strategy for improving the performances of EC energy storage devices (Table 2).

#### 4. Conclusion

We fabricated conductive FTO films via the NaOH effect during USPD. The fresh approach to increasing the F-doping concentration without the extra addition of  $NH_4F$  source was carried out through the chemical reaction between NaOH and HF, which enables the dissociated  $F^-$  from HF to act as a doping source. The increased F-doping concentration of the FTO films through the NaOH effect generated enhanced carrier concentration as well as surface densification that was beneficial to Hall mobility, resulting in a lower  $R_{sh}$  of the FTO films. As a result of the improved conduction in the FTO films fabricated with the volume percentage of 5 vol%, the films showed enhanced EC performances, fast switching speeds (6.6 s for coloration speed and 5.4 s for bleaching speed) and a superb CE (58.1  $cm^2/C$ ). The fast switching speeds were caused by the accelerated  $Li^+$  and electron transport in the active electrodes due to the decreased  $R_{sh}$  and superb CE value was generated from the broadened  $\Delta T$  as an effect of increased electrochemical activity. In addition to the EC performance, the enhanced electrochemical activity induced by the decreased  $R_{sh}$  of the FTO films to cause an efficient transport of large quantity of  $Li^+$  and electrons into the active electrodes brought about improved energy storage performance, a higher specific capacitance (65.2 F/g at 2 A/g). Therefore, the NaOH effect can be a valuable means to improve the F-doping on FTO films thereby escaping their chronic weakness to improve the performance of EC energy storage devices.

#### Declaration of competing interest

The authors declare that they have no known competing financial interests or personal relationships that could have appeared to influence the work reported in this paper.

#### Acknowledgements

This work was supported by the National Research Foundation of Korea (NRF) grant funded by the Korea government (MSIT) (No. 2019R1 A2 C1005836).

#### References

- [1] H. Aliasghari, A.M. Arabi, H. Haratizadeh, A novel approach for solution combustion synthesis of tungsten oxide nanoparticles for photocatalytic and electrochromic applications, *Ceram. Int.* 46 (2020) 403–414.
- [2] B.-R. Koo, M.-H. Jo, K.-H. Kim, H.-J. Ahn, Multifunctional electrochromic energy

- storage devices by chemical cross-linking: impact of a  $\text{WO}_3\cdot\text{H}_2\text{O}$  nanoparticle-embedded chitosan thin film on amorphous  $\text{WO}_3$  films, *NPG Asia Mater.* 12 (2020) 10.
- [3] G. Cai, P. Darmawan, M. Cui, J. Wang, J. Chen, S. Magdassi, P.S. Lee, Highly stable transparent conductive silver grid/PEDOT:PSS electrodes for integrated bifunctional flexible electrochromic supercapacitors, *Adv. Energy Mater.* 6 (2016) 1501882.
  - [4] J. Wang, L. Zhang, L. Yu, Z. Jiao, H. Xie, X.W. Lou, X.W. Sun, A bi-functional device for self-powered electrochromic window and self-rechargeable transparent battery applications, *Nat. Commun.* 5 (2014) 4921.
  - [5] G. Cai, J. Wang, P.S. Lee, Next-generation multifunctional electrochromic devices, *Accounts Chem. Res.* 49 (2016) 1469–1476.
  - [6] K.-H. Kim, B.-R. Koo, H.-J. Ahn, Sheet resistance dependence of fluorine-doped tin oxide films for high-performance electrochromic devices, *Ceram. Int.* 44 (2018) 9408–9413.
  - [7] S. Sarker, H.W. Seo, Y.-K. Jin, Md A. Aziz, D.M. Kim, Transparent conducting oxides and their performance as substrates for counter electrodes of dye-sensitized solar cells, *Mater. Sci. Semicond. Process.* 93 (2019) 28–35.
  - [8] B.-R. Koo, J.-W. Bae, H.-J. Ahn, Low-temperature conducting performance of transparent indium tin oxide/antimony tin oxide electrodes, *Ceram. Int.* 43 (2017) 6124–6129.
  - [9] B.-R. Koo, D.-H. Oh, H.-J. Ahn, Influence of Nb-doped  $\text{TiO}_2$  blocking layers as a cascading band structure for enhanced photovoltaic properties, *Appl. Surf. Sci.* 433 (2018) 27–34.
  - [10] K.-H. Kim, B.-R. Koo, H.-J. Ahn, Effects of Sb-doped  $\text{SnO}_2\text{-WO}_3$  nanocomposite on electrochromic performance, *Ceram. Int.* 45 (2019) 15990–15995.
  - [11] M.-H. Jo, B.-R. Koo, H.-J. Ahn, Fe co-doping effect on fluorine doped tin oxide transparent conducting films accelerating electrochromic switching performance, *Ceram. Int.* 46 (2020) 10578–10584.
  - [12] A.V. Moholkar, S.M. Pawar, K.Y. Rajpure, C.H. Bhosale, J.H. Kim, Effect of fluorine doping on highly transparent conductive spray deposited nanocrystalline tin oxide thin films, *Appl. Surf. Sci.* 255 (2009) 9358–9364.
  - [13] J. Wang, S. Liu, X. Cao, Z. Wang, Y. Guo, X. Li, C. Liu, W. Jiang, H. Wang, N. Wang, S. Wu, H. Tao, W. Ding, One-pot synthesis and gas sensitivity of  $\text{SnO}_2$  nanoparticles prepared using two Sn salts of  $\text{SnCl}_4\cdot 5\text{H}_2\text{O}$  and  $\text{SnCl}_2\cdot 2\text{H}_2\text{O}$ , *Appl. Phys. Mater. Sci. Process* 126 (2020) 44.
  - [14] B.-R. Koo, J.-W. Bae, H.-J. Ahn, Optoelectronic multifunctionality of combustion-activated fluorine-doped tin oxide films with high optical transparency, *Ceram. Int.* 45 (2019) 10260–10268.
  - [15] C. Agashe, S. Mahamuni, Competitive effects of film thickness and growth rate in spray pyrolytically deposited fluorine-doped tin dioxide films, *Thin Solid Films* 518 (2010) 4868–4873.
  - [16] E.-B. Ko, J.-S. Choi, H. Jung, S.-C. Choi, C.-Y. Kim, Low temperature synthesis of fluorine-doped tin oxide transparent conducting thin film by spray pyrolysis deposition, *J. Nanosci. Nanotechnol.* 16 (2016) 1934–1937.
  - [17] S.J. Ikhmayies, R.N. Ahmad-Bitar, Using HF rather than  $\text{NH}_4\text{F}$  as doping source for spray-deposited  $\text{SnO}_2\text{:F}$  thin films, *J. Cent. South Univ.* 19 (2012) 791–796.
  - [18] Z.-Z. Xie, Y.-S. Ong, J.-L. Kuo, On the effects of basis-set in studying the hydration and dissociation of HF in cubic  $\text{HF}(\text{H}_2\text{O})_7$  clusters, *Chem. Phys. Lett.* 453 (2008) 13–17.
  - [19] M.E. Guendouzi, J. Faridi, L. Khmar, Chemical speciation of aqueous hydrogen fluoride at various temperatures from 298.15 K to 353.15 K, *Fluid Phase Equil.* 499 (2019) 112244.
  - [20] B.-R. Koo, D.-H. Oh, D.-H. Riu, H.-J. Ahn, Improvement of transparent conducting performance on oxygen-activated fluorine-doped tin oxide electrodes formed by horizontal ultrasonic spray pyrolysis deposition, *ACS Appl. Mater. Interfaces* 9 (2017) 44584–44592.
  - [21] N. Haddad, Z. Ben Ayadi, H. Mahdhi, K. Djessas, Influence of fluorine doping on the microstructure, optical and electrical properties of  $\text{SnO}_2$  nanoparticles, *J. Mater. Sci. Mater. Electron.* 28 (2017) 15457–15465.
  - [22] B. Zhang, Y. Tian, J.X. Zhang, W. Cai, The role of oxygen vacancy in fluorine-doped  $\text{SnO}_2$  films, *Physica B* 406 (2011) 1822–1826.
  - [23] B.-R. Koo, J.-W. Bae, H.-J. Ahn, Percolation effect of  $\text{V}_2\text{O}_5$  nanorod/graphene oxide nanocomposite films for stable fast-switching electrochromic performances, *Ceram. Int.* 45 (2019) 12325–12330.
  - [24] A. Benhaoua, A. Rahal, B. Benhaoua, M. Jlassi, Effect of fluorine doping on the structural, optical and electrical properties of  $\text{SnO}_2$  thin films prepared by spray ultrasonic, *Superlattice. Microsc.* 70 (2014) 61–69.
  - [25] A.P. Roth, J.B. Webb, D.F. Williams, Absorption edge shift in ZnO thin films at high carrier densities, *Solid State Commun.* 39 (1981) 1269–1271.
  - [26] L. Chinnappa, K. Ravichandran, K. Saravanakumar, G. Muruganatham, B. Sakthivel, The combined effects of molar concentration of the precursor solution and fluorine doping on the structural and electrical properties of tin oxide films, *J. Mater. Sci. Mater. Electron.* 22 (2011) 1827–1834.
  - [27] B.L. Zhu, F. Liu, K. Li, K. Lv, J. Wu, Z.H. Gan, J. Liu, D.W. Zeng, C.S. Xie, Sputtering deposition of transparent conductive F-doped  $\text{SnO}_2$  (FTO) thin films in hydrogen-containing atmosphere, *Ceram. Int.* 43 (2017) 10288–10298.
  - [28] B.L. Zhu, X. Zhao, W.C. Hu, T.T. Li, J. Wu, Z.H. Gan, J. Liu, D.W. Zeng, C.S. Xie, Structural, electrical, and optical properties of F-doped  $\text{SnO}$  or  $\text{SnO}_2$  films prepared by RF reactive magnetron sputtering at different substrate temperatures and  $\text{O}_2$  fluxes, *J. Alloys Compd.* 719 (2017) 429–437.
  - [29] T. Yamada, H. Makino, N. Yamamoto, T. Yamamoto, Ingrain and grain boundary scattering effects on electron mobility of transparent conducting polycrystalline Ga-doped ZnO films, *J. Appl. Phys.* 107 (2010) 123534.
  - [30] B.-R. Koo, H.-J. Ahn, Effect of hybrid nanoinks on solution-based Sn-doped  $\text{In}_2\text{O}_3$  films under low-temperature microwave annealing, *Ceram. Int.* 42 (2016) 509–517.
  - [31] A.P. Roth, J.B. Webb, D.F. Williams, Band-gap narrowing in heavily defect-doped ZnO, *Phys. Rev. B* 25 (1982) 7836–7839.
  - [32] B.-R. Koo, K.-H. Kim, H.-J. Ahn, Novel tunneled phosphorous-doped  $\text{WO}_3$  films achieved using ignited red phosphorous for stable and fast switching electrochromic performances, *Nanoscale* 11 (2019) 3318–3325.
  - [33] Y. Yao, Q. Zhao, W. Wei, Z. Chen, Y. Zhu, P. Zhang, Z. Zhang, Y. Gao,  $\text{WO}_3$  quantum-dots electrochromism, *Nanomater. Energy* 68 (2020) 104350.
  - [34] B.-R. Koo, H.-J. Ahn, Research impact on emerging quantum materials for electrochromic applications, *Isr. J. Chem.* 59 (2019) 673–678.
  - [35] J. Pan, R. Zheng, Y. Wang, X. Ye, Z. Wan, C. Jia, X. Weng, J. Xie, L. Deng, A high-performance electrochromic device assembled with hexagonal  $\text{WO}_3$  and NiO/PB composite nanosheet electrodes towards energy storage smart window, *Sol. Energy Mater. Sol. Cells* 207 (2020) 110337.
  - [36] Y.-H. Lee, J.S. Kang, J.-H. Park, J. Kang, I.-R. Jo, Y.-E. Sung, K.-S. Ahn, Color-switchable electrochromic  $\text{Co}(\text{OH})_2/\text{Ni}(\text{OH})_2$  nanofilms with ultrafast kinetics for multifunctional smart windows, *Nanomater. Energy* 72 (2020) 104720.